RNA Isolation and RT-PCR Analysis

Total RNA was extracted from embryos at 24 hr post-fertilization (hpf) with TRIzol reagent according to the manufacturer's (Life Technologies) protocol. Double-stranded cDNA was synthesized with M-MLV reverse transcriptase (Promega) and then amplified by PCR with ExTaq (Takara). For detecting the splicing mutation (caused by the MO injections) in *nup107* exon 24, the following primers were used: 5′-TGAACTGTCCTCCGGTGAAG-3′ (forward) and 5′-TGCGATGATGTCAGCAAGAC-3′ (reverse). For the PCR amplifications, the initial denaturing step at 94°C for 5 min was followed by 29 cycles of 30 s at 94°C, 30 s at 61°C, 30 s at 72°C, and a final extension of 7 min at 72°C. PCR products were separated on 3% agarose gels.

Histopathology and Transmission Electron Microscopy of Zebrafish

Larvae injected with control MO, *nup107*-TB MO, and *nup107*-SB MO at 5.5 days after fertilization were fixed with 2% paraformaldehyde and 2% glutaraldehyde in 0.1 M cacodylate buffer (pH 7.4) at 4°C overnight. After fixation, the samples were washed three times with 0.1 M cacodylate buffer for 30 min each and then postfixed with 2% osmium tetroxide in 0.1 M cacodylate buffer at 4°C for 3 hr. The samples were dehydrated in graded ethanol solution (50%, 70%, 90%, and 100%), infiltrated with propylene oxide (PO) two times for 30 min each, immersed in a 70:30 mixture of PO and resin (Quetol-812, Nisshin EM) for 1 hr, and then kept in an open-capped tube so that volatile PO would evaporate overnight. The samples were transferred to fresh 100% resin and polymerized at 60°C for 48 hr. The polymerized resins were cut into semi-thin (1.5-μm) sections with an Ultracut UCT (Leica) and then stained with 0.5% toluidine blue. Ultra-thin (70-nm) sections were cut on an Ultracut UCT (Leica) ultramicrotome and mounted on copper grids. The sections were stained with 2% uranyl acetate at room temperature for 15 min, washed with distilled water, and stained with lead stain solution (Sigma-Aldrich) at room temperature for 3 min. The grids were observed with a transmission electron microscope (JEM-1400Plus, JEOL) at 80 kV.

Molecular-Dynamics Simulation of the p.Asp831Ala Substitution in NUP107

Molecular-dynamics (MD) simulations of the wild-type and p.Asp831Ala Nup107 were carried out with the program package GROMACS (Groningen Machine for Chemical Simulation) version 5.0 with the Optimized Potentials for Liquid Simulations all-atom force field based on the local Møller-Plesset perturbation theory (OPLS-AA/L).[21] The starting structure of NUP107 was extracted from the crystal structure of the NUP107-NUP133 complex (PDB: 3CQC). The missing regions in NUP107 were modeled with the Phyre2 modeling server,[22] and the p.Asp831Ala substitution was introduced with FoldX software.[23] The wild-type and altered NUP107 molecules were solvated with simple-point-charge water molecules in a cubic box extending at least 1.0 nm from the protein surface. Sodium ions were added to neutralize the systems, which were then subjected to energy minimization for 50,000 steps by steepest descent. The minimized systems were then equilibrated by position-restrained MD simulation for soaking the water molecules in the macromolecules in two steps as follows: an NVT ensemble (constant number of particles, volume, and temperature) for 100 ps and an NPT ensemble (constant number of particles, pressure, and temperature) for 4,000 ps each at 310 K. The well-equilibrated systems were then subjected to MD simulations for 30 ns each at 310 K without any restrictions. In all simulations, for maintaining a constant temperature of 310 K, temperature coupling using velocity rescaling with a stochastic term[24] was employed with a coupling constant τ of 0.1 ps. Van der Waals interactions were modeled with 6–12 Lennard-Jones potentials with a 1.4-nm cutoff. Long-range electrostatic interactions were calculated with the particle-mesh Ewald method[25] with a 1.4-nm cutoff for the real-space term. Covalent bonds were constrained with the LINCS algorithm.[26]

Results

Pathogenic Mutations Detected by WES

To identify the genetic cause of early-onset SRNS, we performed WES on 18 probands. Because we found multiple affected siblings in ten families, we speculated on an autosomal-recessive inheritance pattern for SRNS and focused on the recessive variants shared by two or more families with well-performed WES data (Tables S1–S3, S4, and S5). Biallelic mutations in *NUP107*, which encodes NUP107, were common in five families, and the mutation co-segregated perfectly with the affected state in all five families (Figure 1A, Table 1, and Figure S1). None of the other families in our cohort had any pathological variants in *NUP107* or any other known genes associated with SRNS, as listed in Table S6.

We identified a total of four *NUP107* mutations, including two missense mutations (c.469G>T [p.Asp157Tyr] and c.2492A>C [p.Asp831Ala]), one 5-bp deletion (c.1079_1083delAAGAG [p.Glu360Glyfs*6]), and one splice-donor-site mutation (c.969+1G>A) (Table 2). Heterozygous c.2492A>C was common in all five families. The two missense mutations altered evolutionally conserved amino acids (Figure S2) and were predicted to be pathogenic by web-based programs PolyPhen-2 and MutationTaster (Table 2). Furthermore, p.Asp831Ala resides within the Nup84-Nup100 domain (Figure S3). The 5-bp deletion was subjected to nonsense-mediated mRNA decay and probably led to a lack of protein synthesis (Figure S4). The splicing mutation (c.969+1G>A) causes a loss of the intrinsic splicing donor site (Figure S5). All four variants were examined in the EVS, ExAC Browser, HGVD, and in-house Japanese exome database (n = 575). The c.1079_1083delAAGAG variant was observed at frequencies of 0.0000083 in the ExAC Browser and 0.0008696 in the in-house Japanese exome data. Another variant, c.2492A>C, was observed at a frequency of 0.0013587 only in HGVD, but not in the EVS, ExAC Browser, or in-house Japanese exome data (Table 2). The other mutations (c.469G>T and c.969+1G>A) were never observed in any of four variant databases. Among 881 *NUP107* variants registered in the ExAC Browser, a total of 31 variants with a MAF $\geq$ 0.005 were in non-coding regions (intronic but not in canonical acceptor or donor sites or UTRs) or were synonymous variants (Table S7). Furthermore, 36 loss-of-function variants in *NUP107* are not homozygous (all heterozygous; Table S8). Therefore, this genetic

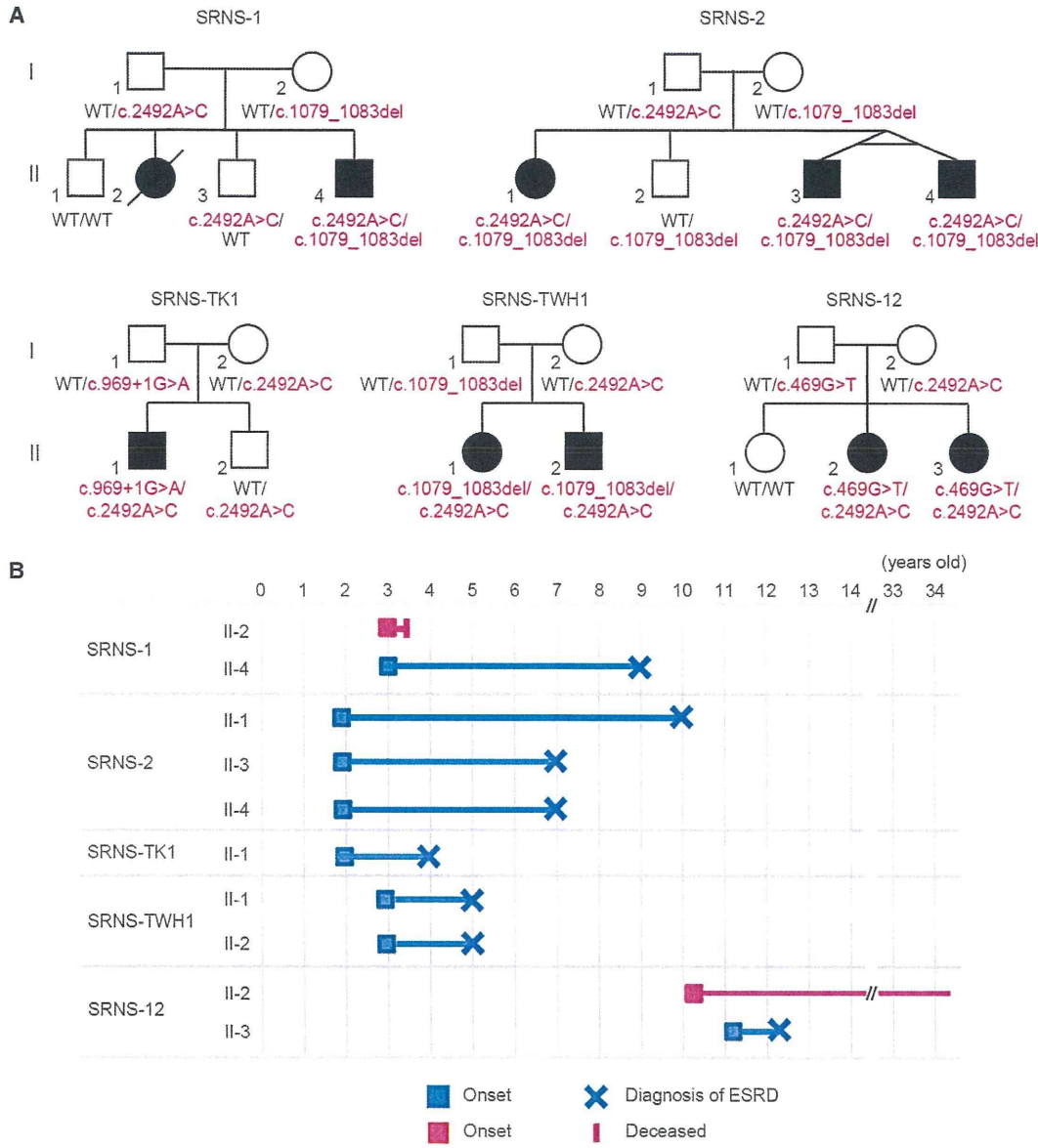

Figure 1. Genetic Analysis and Clinical Course of Early-Onset SRNS in Affected Individuals with *NUP107* Mutations
(A) Familial pedigrees and *NUP107* mutations. Mutant alleles are colored in red. WT indicates the wild-type allele. Filled and unfilled symbols represent affected and unaffected members, respectively.
(B) Clinical course of the affected individuals. The onset of renal symptoms and diagnosis of ESRD are represented by squares and crosses, respectively. Blue and red horizontal bars indicate the period leading to ESRD and the period before completed ESRD, respectively. SRNS-1 II-2 died from a viral infection before the advent of ESRD.

evidence strongly suggests that biallelic *NUP107* mutations could lead to autosomal-recessive SRNS.

A Common Haplotype Harboring c.2492A>C

Interestingly, all affected individuals carry c.2492A>C heterozygously. To determine whether c.2492A>C was derived from an ancestral chromosome, we constructed the haplotype in all families by using informative microsatellite markers and SNPs. We confirmed that a 412-kb haplotype was shared by all five families (Figure S6). Considering the extreme rarity of c.2492A>C in different whole-exome databases, c.2492A>C is likely to be specific to East Asians.

Clinical Characterization of NUP107-Related SRNS

Noticeably, the clinical course of affected individuals with *NUP107* mutations was similar (Figure 1B and the supplemental note). In brief, the four families consistently showed early-onset SRNS whereby NS first manifested itself at age 2–3 years and ESRD became evident before age 10

Table 1. Clinical and Genetic Summary of SRNS-Affected Families Harboring *NUP107* Mutations

Family	Individual	Mutation	Age at Onset (Years)	Age at Diagnosis of ESRD (Years)	Treatment	Histology (Subtype, Age in Years)
SRNS-1[a]	II-2[b]	ND	3	NA	Pred	FSGS (NOS, 3)
	II-4	c.[1079_1083del];[2492A>C]	3	9	Pred, CyA, CPA	FSGS (NOS, 3)
SRNS-2[a]	II-1	c.[1079_1083del];[2492A>C]	2	10	Pred, CPA	MCNS (NOS, 2), FSGS (NOS, 4)
	II-3	c.[1079_1083del];[2492A>C]	2	7	Pred	MCNS (2)
	II-4	c.[1079_1083del];[2492A>C]	2	7	Pred	FSGS (NOS, 2)
SRNS-TK1	II-1	c.[969+1G>A];[2492A>C]	2	4	Pred, CyA, CPA	FSGS (NOS, 2)
SRNS-TWH1	II-1	c.[1079_1083del];[2492A>C]	3	5	Pred, ARB, PP	FSGS (collapsing, 3)
	II-2	c.[1079_1083del];[2492A>C]	3	5	Pred, CyA, ARB	FSGS (collapsing, 3)
SRNS-12[a]	II-2	c.[469G>T];[2492A>C]	10	NA	ARB	ND
	II-3	c.[469G>T];[2492A>C]	11	12	Pred, ARB	FSGS (NOS, 11)

Abbreviations are as follows: ARB, AT II receptor blocker; collapsing, collapsing variants; CPA, cyclophosphamide; CyA, cyclosporine A; ESRD, end-stage renal disease; FSGS, focal segmental glomerulosclerosis; MCNS, minimal-change nephrotic syndrome; NA, not applicable; ND, not determined; NOS, non-specific type; PP, plasmapheresis; Pred, prednisone.
[a]These families appear in a previous report by Kitamura et al.[12]
[b]This individual died from a viral infection at the age of 3 years.

years. One family (SRNS-12) showed an exceptionally late onset of NS, which appeared after 10 years of age, and renal function has been relatively preserved at the current 34 years of age. Renal biopsies revealed histopathological FSGS in all affected individuals (Figure 2, Table 1, and Figure S7). Depletion of NUP107 was shown to lead to apoptosis in eukaryotes,[20,27] and we observed apoptotic changes in the renal biopsy samples from SRNS individuals (SRNS-TWH1 II-1 and II-2) with *NUP107* mutations. Cells with the characteristic morphological features, such as nuclear shrinkage and fragmentation, were occasionally found in the glomeruli and renal tubules (Figure S8). Some of these cells could be TUNEL positive (apoptotic), although we failed to recognize TUNEL-positive cells in the glomeruli of the few biopsied specimens, given that only ten glomeruli were observed (data not shown). Among them, five individuals underwent renal transplants and have experienced no recurrence of SRNS to date. Additionally, none of them showed neurological phenotypes.

NUP107 Function and *NUP107* Expression in Humans

NUP107 is an essential component of the NPC, which is one of the largest protein complexes (~125 MDa in vertebrates) in eukaryotes and comprises ~30 nucleoporins embedded in the nuclear envelope.[28,29] It facilitates the efficient transfer of macromolecules between the nucleus and cytoplasm in a highly selective manner and plays pivotal roles in the nuclear framework and gene expression.[28,30–33] Although some nucleoporins have tissue specificity,[34] *NUP107* and NUP107 are ubiquitously expressed as the core gene and the essential scaffold protein, respectively, of the NPC.[29,35–37] As the results of the TaqMan expression assay show, *NUP107* is expressed ubiquitously in most human fetal and adult tissues, including the kidney (Figure S9). To evaluate the physiological relevance of NUP107 in human podocytes, we examined the intracellular localization of NUP107, along with WT1 (a podocyte-specific transcription factor[38]) and Ezrin (a marker protein for apical domains of epithelial cells[39]), in human podocytes. Confocal microscopy demonstrated that NUP107 co-localized with WT1 and was distributed in a speckle-like pattern in the nuclei of human podocytes surrounding the glomerular capillary tufts (Figure S10). In addition to podocytes, most other cell types showed a similar staining pattern for NUP107. These data suggest that NUP107 has an important function for renal filtration in human podocytes. A direct link between NUP107 and renal disease has never been shown, but *NUP107* knockdown in HeLa cells altered the localization of ELYS, and this affected the proper localization of lamin A/C,[19] an alteration in which caused FSGS.[40]

Effect of the Common NUP107 p.Asp831Ala Substitution on the Structure of the Protein and Its Binding to NUP133

To evaluate the effect of p.Asp157Tyr and p.Asp831Ala substitutions from a structural viewpoint, we mapped the variant positions on the crystal structure of the yeast Sec13-Nup145C-Nup84 complex (PDB: 3IKO),[41] which is analogous to the human SEC13-NUP96-NUP107 complex (NUP96 is the C-terminal half product of *NUP98* [GenBank: NM_016320.4; MIM: 601021], processed after translation[42,43]) and the human NUP107-NUP133 complex (PDB: 3CQC).[14] Asp157 is predicted to reside on the surface of the protein, suggesting that the p.Asp157Tyr substitution does not affect the folded structure of NUP107 (Figure S11). However, because this protein interacts with many other proteins,[44] the possibility that the p.Asp157Tyr substitution might impair these interactions cannot be excluded, although no such changed

Table 2. *NUP107* Mutations in Affected Individuals with Early-Onset SRNS

Mutation	Amino Acid Change	PolyPhen-2	PyloP	MutationTaster	Grantham	EVS	ExAC	HGVD	In-House Exomes[a] (n = 575)
c.469G>T	p.Asp157Tyr	0.712	2.84	0.998403	160	0	0	0	0
c.969+1G>A	splice site	NA	NA	NA	NA	0	0	0	0
c.1079_1083delAAGAG	p.Glu360Glyfs*6	NA	NA	NA	NA	0	0.0000083	0	0.0008696
c.2492A>C	p.Asp831Ala	1.000	1.952	0.99995	126	0	0	0.0013587	0

Mutations were annotated according to *NUP107* cDNA (GenBank: NM_020401.2). Abbreviations are as follows: EVS, NHLBI Exome Sequencing Project Exome Variant Server; HGVD, Human Genetics Variation Database (the public exome database of the Japanese population).
[a]In-house exome database of Japanese control individuals.

interaction for this particular variant site has been reported. Because the Asp831 side chain forms hydrogen bonds with the Arg842 side chain, the p.Asp831Ala substitution is considered to disrupt these hydrogen bonds. To evaluate the effects of this variant on the structure of NUP107, we performed MD simulations for wild-type and altered NUP107 in solution. In this substitution, a region around the variant site and a region involved in interactions with NUP133 (amino acid residues 881–890) both showed more fluctuations than did those same regions in the wild-type protein (Figure S12). This NUP133-interacting region is considered to be structurally correlated with the variant site through van der Waals contacts (Figure S12B). The results from the MD simulations suggest that the p.Asp831Ala substitution impairs the molecular interaction between NUP107 and NUP133.

Impaired Function of the Altered NUP107

Because NUP107 interacts with NUP133 via its C-terminal tail,[14] we investigated the mutational effects on the protein-protein interaction between NUP107 and NUP133 in vitro. We used an in vitro pull-down assay with recombinant proteins produced in a wheat germ cell-free system to determine the contribution of the C-terminal region of NUP107. Consistent with a previous report,[14] the altered NUP107 that lacked a third of the C-terminal region (amino acids 645–925) did not bind to NUP133 as tightly as wild-type NUP107 under equilibrium conditions (Figure S13). Likewise, two truncated NUP107 proteins with extensively shorter C termini (p.Asp324* and p.Glu360Glyfs*6) also showed weaker binding to NUP133. Notably, a p.Asp831Ala protein with an altered C terminus exhibited significantly reduced binding to NUP133, whereas a p.Asp157Tyr protein with an altered N terminus retained full binding activity (Figure 3A). Wild-type GFP-fused NUP107, which was transiently produced by a mammalian expression vector, was bound to endogenous NUP133 in HeLa cells, and the p.Asp831Ala protein was also bound to NUP133 but weakly in comparison to the wild-type (Figure 3B). Observation of the intracellular localization of altered GFP-NUP107 indicated that the two truncated proteins were distributed mainly in the cytoplasm, whereas the wild-type protein was clearly localized in the nuclear envelope (Figure 3C). The p.Asp831Ala altered protein was localized in the nuclear envelope and cytoplasm (Figure 3C). These results are consistent with the impaired interaction observed between the altered NUP107 and NUP133.

Zebrafish with *nup107* Knockdown Have Glomerular Abnormalities Mimicking SRNS

Reportedly, zebrafish with homozygous *nup107* mutations and morphants with *nup107* knockdown produced with anti-sense MOs each similarly showed a thin pharyngeal skeleton, unfolded intestine, and loss of swim bladder and died on days 5 and 6.[20] However, the specific renal phenotype was not investigated. Therefore, we injected the *nup107*-TB MO or *nup107*-SB MO to create an in-frame (15-bp) deletion at exon 24 to mimic the commonly shared missense mutation (c.2492A>C [p.Asp831Ala]) and then carefully observed the renal phenotype in vivo (Figures S14 and S15). As reported previously,[20] neither of the zebrafish morphants developed edema until they died at around days 5 and 6 (Figure S14A). Furthermore, we sought to identify the glomerular filtration impairment in knockdown zebrafish (*nup107*-TB MO) but did not observe any traces of recognizable protein leakage in glomeruli at 96 hpf (data not shown). Although zebrafish might not be the best animal model for generating renal phenotypes, in a microscopic section of the *nup107*-SB morphant, we were able to find supportive findings in that the glomeruli were generally underdeveloped and showed hypoplastic or poorly organized capillary vessels and mesangial regions (Figures S14C–S14E). Electron microscopy revealed abnormally shaped foot processes and collapse of the capillary lumen in both morphants (Figures S14F–S14K and S16). Because these observations are similar to those from humans with FSGS, the zebrafish morphants might reflect the renal changes caused by the *NUP107* mutation.

Unchanged NPC Localization in Lymphoblastoid Cells from Affected Individuals with *NUP107* Mutations

Reportedly, NUP107 depletion results in decreased or absent NPCs.[29,36] However, a lymphoblastoid cell line derived from affected individuals showed no apparent NPC loss or abnormality by immunohistochemistry analysis (data not shown), which indicates that some residual

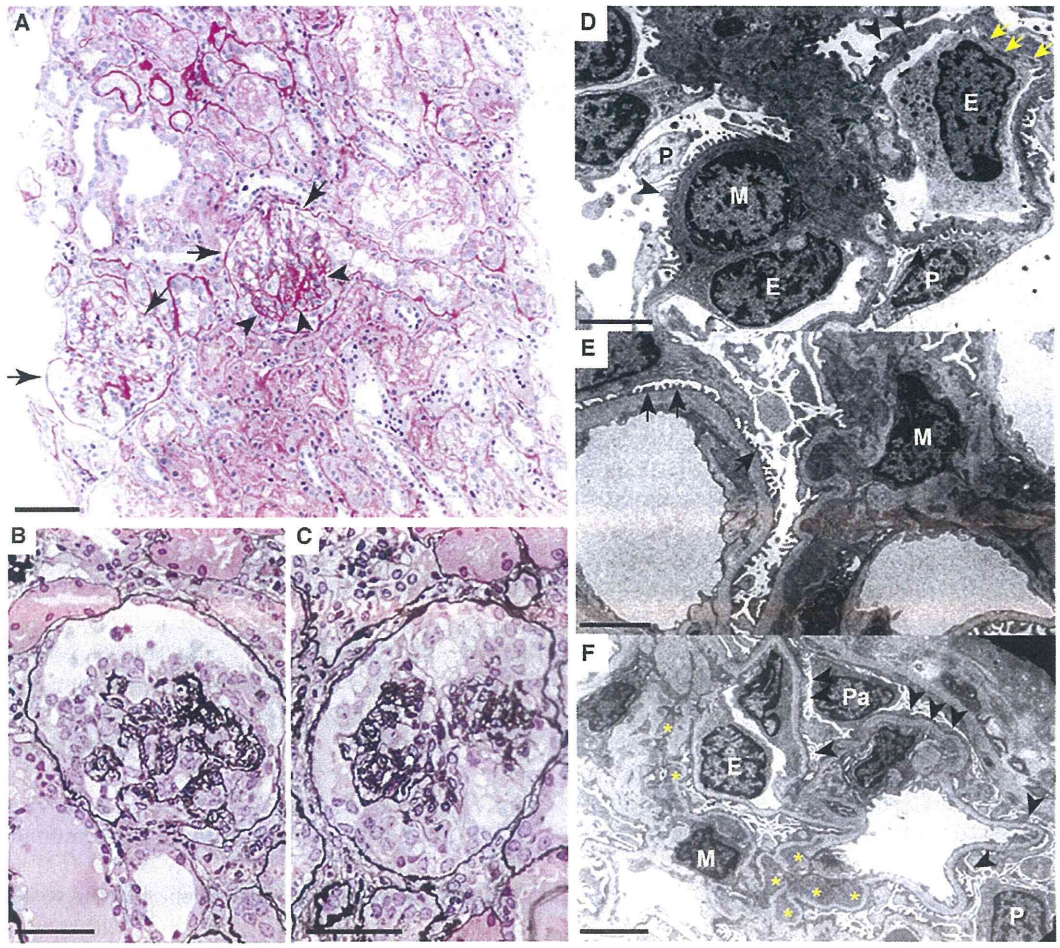

Figure 2. Kidney Histopathology of Affected Individuals with Biallelic *NUP107* Mutations
(A–C) Light micrographs of kidney biopsy specimens from SRNS-TWH II-1. (A) A low-power view (periodic acid-Schiff stain, 100× magnification) of two representative abnormal glomeruli (arrows). Half of the glomerulus is sclerosed (arrowheads). (B and C) Enlarged images (periodic acid methenamine silver stain, 400× magnification) show the collapse of glomerular tufts with hypertrophy and hyperplasia of the glomerular epithelial cells that fill the urinary space. Tubular injury accompanying atrophy of epithelia and interstitial fibrosis is noted.
(D–F) Electron micrographs of biopsy specimens from SRNS-2 II-1 (D), SRNS-2 II-3 (E), and SRNS-2 II-4 (F). Effacement of podocyte foot processes and some mesangial expansion with sub-endothelial electron-dense deposits are apparent. The thickness of the glomerular basement membrane appears normal and shows no evidence of splitting, lamellation, or fragmentation, thereby excluding the possibility of a primary basement-membrane defect. Accumulation of storage materials and dysmorphic mitochondria were not found in the podocyte cytoplasm. Abbreviations are as follows: E, endothelial cell; M, mesangial cell; P, podocyte; Pa, papillary epithelia. Arrowheads indicate effacement of podocyte foot processes, yellow arrows represent electron dense deposits, black arrows show flattened podocyte foot processes, and yellow asterisks show paramesangial deposits.
Scale bars represent100 μm (A), 40 μm (B and C), 2 μm (D and E), and 5 μm (F).

functions of altered NUP107 might persist in the cells of affected individuals, at least under non-stressful conditions. NUP107 is an essential scaffold protein in the NPC, a structure that is evolutionary conserved from yeast to vertebrates.[29,36] Therefore, in the null state, *NUP107* mutants might be lethal in humans.

Discussion

In this study, we have shown that biallelic *NUP107* mutations cause early-onset SRNS in humans. Affected individuals with *NUP107* mutations usually developed SRNS at 2–3 years of age and progressed to ESRD before 10 years of age but experienced no recurrence of the disease after renal transplantation. How do *NUP107* mutations cause a glomerular phenotype in humans? This might be partly explained by the specific properties of podocytes, which are highly differentiated with a unique architecture (foot processes and slit membranes).[45,46] In affected individuals with *NUP107* mutations, insufficient NUP107 function could cause immature and/or hypoplastic podocytes, or at least functionally impaired podocytes that are progressively destroyed by

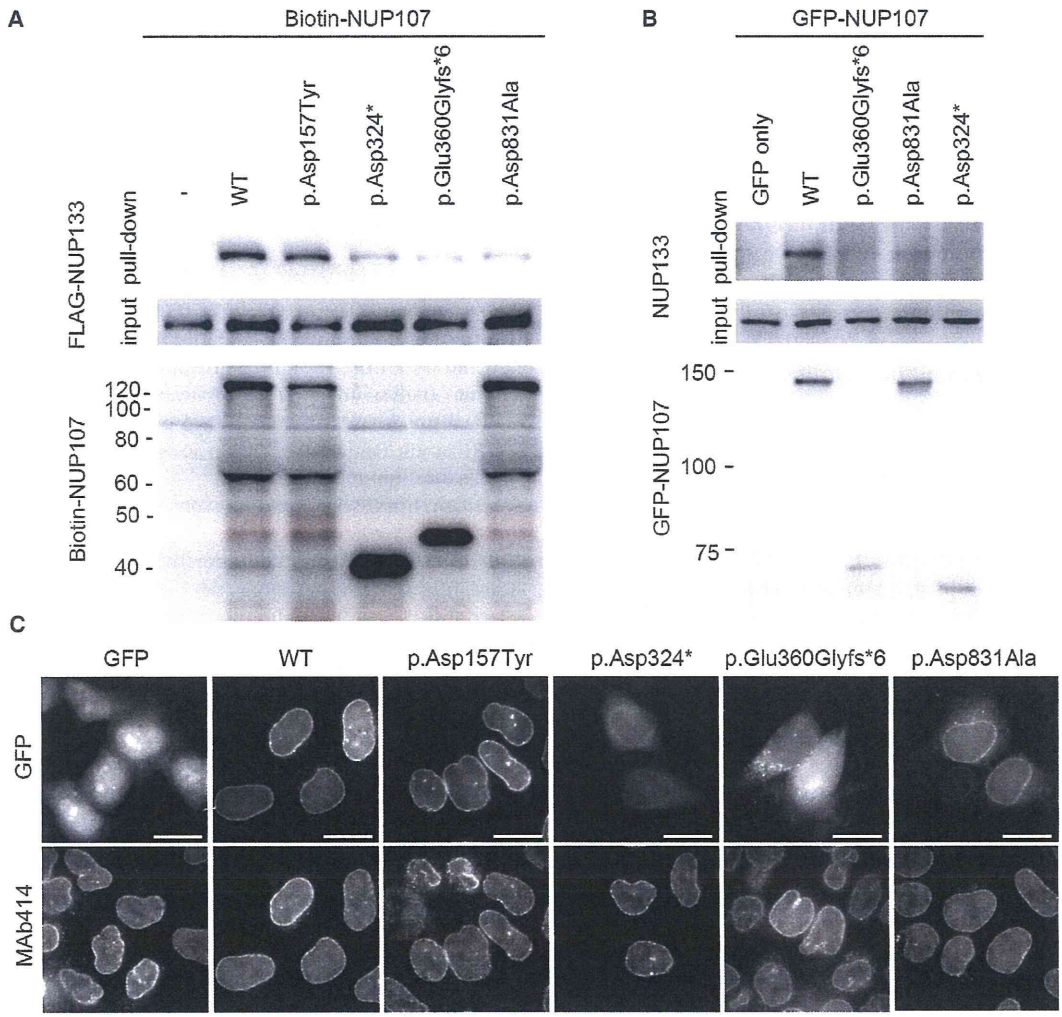

Figure 3. Decreased Intermolecular Interactions between NUP107 and NUP133
(A) In vitro protein-protein binding assay of altered NUP107 with NUP133. The FLAG-tagged NUP133 mixed with biotinylated altered NUP107 proteins was subjected to a pull-down assay with streptavidin magnetic beads. The bound proteins were separated by SDS-PAGE and then detected with an anti-FLAG antibody or with streptavidin-horseradish peroxidase. The corresponding protein inputs are shown in the middle and bottom panels.
(B) Evaluation of the interaction between NUP107 and NUP133 with the use of wild-type NUP107 and its alterations. Wild-type GFP-NUP107 or its alterations were transiently produced in HeLa cells and precipitated with an anti-GFP antibody. The NUP107-NUP133 interaction was analyzed via immunoblotting using the antibodies indicated.
(C) Subcellular localization of NUP107 or its alterations. For visualizing localization of altered or wild-type GFP-NUP107 in HeLa cells, the cells were fixed and stained with a MAb414 antibody recognizing the NPC on the nuclear envelopes. Scale bars represent 20 μm.
The following abbreviation is used: WT, wild-type.

increased filtration pressure after birth. Interestingly, nuclear-envelope proteins, including NPCs, are closely associated with mechanotransduction signaling,[47,48] and mechanical stretching decreases podocyte proliferation and cell-body size by reorganizing the actin cytoskeleton in vitro.[49,50] Thus, increased post-natal capillary pressure leading to mechanical stretching of vulnerable podocytes might accelerate glomerulus damage. Furthermore, mature podocytes do not regenerate.[51,52] Thus, the core pathological condition of SRNS caused by *NUP107* mutations is a structural abnormality, which correlates well with the early SRNS onset in childhood, its steroid resistance, and its lack of post-transplant relapse (Figure S17).

Recently, a homozygous missense mutation (c.303G>A [p.Met101Ile]) was reported in an affected individual who is from a consanguineous family and presents with global developmental delay and early-onset FSGS.[53] However, none of our affected individuals with *NUP107* recessive mutations show neurological impairment. Additional genetic factors might be involved in the neurological symptoms of the consanguineous family. Alternatively, different mutations could cause an additional neurological phenotype. This mutation has been suggested to lead to

abnormal splicing (and possibly a nearly null function), although no direct evidence has been shown.[53] As for p.Asp157Tyr, we could not find direct evidence of its functional impairment experimentally. However, it could be a hypomorphic variant; if so, this might explain the milder phenotype in the SRNS-12 family, who carries both missense mutations (c.469G>T [p.Asp157Tyr] and c.2492A>C [p.Asp831Ala]). Thus, it is possible that the residual NUP107 function left by missense mutations (including c.469G>T [p.Asp157Tyr]) is related to the late onset age and/or milder severity of the disease. It is intriguing that mutations in *NUP107*, which encodes an essential nucleoporin of the NPC, lead to a kidney-specific disease in humans.

In summary, biallelic *NUP107* mutations cause early-onset SRNS for which renal transplantation is the only effective treatment. Access to genetic information is useful for proper clinical management of NS. Therefore, screening *NUP107* mutations in SRNS individuals with broad ranges of clinical severity is strongly encouraged. Furthermore, we did not identify the genetic cause in six pairs of affected siblings and seven single affected individuals in our cohort, which implies a heterogenetic etiology for early-onset SRNS. Further research is necessary to uncover the whole picture of this type of SRNS.

Supplemental Data

Supplemental Data include a supplemental note, 17 figures, and 8 tables and can be found with this article online at http://dx.doi.org/10.1016/j.ajhg.2015.08.013.

Acknowledgments

We are grateful to all the affected individuals and their families who participated in this study. We also thank our clinical colleagues who supported the participating families: Dr. Makoto Endo (Laboratory of Fish Health Management, Tokyo University of Marine Science and Technology) for morphological evaluation of zebrafish and Ms. Sugimoto, Ms. Takabe, and Mr. Mitsui for technical assistance. This work was supported in part by a grant for Research on Measures for Intractable Diseases, a grant for Comprehensive Research on Disability Health and Welfare, and the Strategic Research Program for Brain Science from the Japan Agency for Medical Research and Development; a Grant-in-Aid for Scientific Research on Innovative Areas (Transcription Cycle) (24118007) from the Ministry of Education, Culture, Sports, Science, and Technology of Japan; Grants-in-Aid for Scientific Research (A, B, and C) and for Challenging Exploratory Research from the Japan Society for the Promotion of Science; the fund for Creation of Innovation Centers for Advanced Interdisciplinary Research Areas Program of the Project for Developing Innovation Systems from the Japan Science and Technology Agency; the Takeda Science Foundation; the Osaka Kidney Foundation; and grant HI12C0014 from the Korean Health Technology R&D Project, Ministry of Health & Welfare. K.I. also received grants from Pfizer Japan, Daiichi Sankyo, the Japan Blood Product Organization, Miyarisan Pharmaceutical, AbbVie, CSL Behring, JCR Pharmaceuticals, and Teijin Pharma; and consulting fees from Chugai Pharmaceutical and Astellas Pharma. N.Y. received grants from Novartis Pharma KK and Asahi Kasei Pharma.

Received: June 6, 2015
Accepted: August 28, 2015
Published: September 24, 2015

Web Resources

The URLs for data presented herein are as follows:

1000 Genomes FTP site, ftp://ftp.1000genomes.ebi.ac.uk/vol1/ftp/technical/reference/README.human_g1k_v37.fasta.txt
ExAC Browser, http://exac.broadinstitute.org/
Genome Analysis Toolkit, http://www.broadinstitute.org/gatk
HGVD, http://www.genome.med.kyoto-u.ac.jp/SnpDB/
NHLBI Exome Sequencing Project Exome Variant Server, http://evs.gs.washington.edu/EVS/
Novoalign, http://www.novocraft.com
OMIM, http://www.omim.org
PDB, http://www.rcsb.org/pdb/home/home.do
Picard, http://picard.sourceforge.net
RefSeq, http://www.ncbi.nlm.nih.gov/refseq/
UCSC Genome Browser, https://genome.ucsc.edu/

References

1. Gipson, D.S., Massengill, S.F., Yao, L., Nagaraj, S., Smoyer, W.E., Mahan, J.D., Wigfall, D., Miles, P., Powell, L., Lin, J.J., et al. (2009). Management of childhood onset nephrotic syndrome. Pediatrics *124*, 747–757.
2. Bullich, G., Trujillano, D., Santín, S., Ossowski, S., Mendizábal, S., Fraga, G., Madrid, Á., Ariceta, G., Ballarín, J., Torra, R., et al. (2015). Targeted next-generation sequencing in steroid-resistant nephrotic syndrome: mutations in multiple glomerular genes may influence disease severity. Eur. J. Hum. Genet. *23*, 1192–1199.
3. McKinney, P.A., Feltbower, R.G., Brocklebank, J.T., and Fitzpatrick, M.M. (2001). Time trends and ethnic patterns of childhood nephrotic syndrome in Yorkshire, UK. Pediatr. Nephrol. *16*, 1040–1044.
4. Kim, J.S., Bellew, C.A., Silverstein, D.M., Aviles, D.H., Boineau, F.G., and Vehaskari, V.M. (2005). High incidence of initial and late steroid resistance in childhood nephrotic syndrome. Kidney Int. *68*, 1275–1281.
5. Saleem, M.A. (2013). New developments in steroid-resistant nephrotic syndrome. Pediatr. Nephrol. *28*, 699–709.
6. Zagury, A., Oliveira, A.L., Montalvão, J.A., Novaes, R.H., Sá, V.M., Moraes, C.A., and Tavares, Mde.S. (2013). Steroid-resistant idiopathic nephrotic syndrome in children: long-term follow-up and risk factors for end-stage renal disease. J. Bras. Nefrol. *35*, 191–199.
7. Trautmann, A., Bodria, M., Ozaltin, F., Gheisari, A., Melk, A., Azocar, M., Anarat, A., Caliskan, S., Emma, F., Gellermann, J., et al.; PodoNet Consortium (2015). Spectrum of steroid-resistant and congenital nephrotic syndrome in children: the PodoNet registry cohort. Clin. J. Am. Soc. Nephrol. *10*, 592–600.
8. Lovric, S., Fang, H., Vega-Warner, V., Sadowski, C.E., Gee, H.Y., Halbritter, J., Ashraf, S., Saisawat, P., Soliman, N.A., Kari, J.A., et al.; Nephrotic Syndrome Study Group (2014). Rapid detection of monogenic causes of childhood-onset steroid-resistant nephrotic syndrome. Clin. J. Am. Soc. Nephrol. *9*, 1109–1116.

9. Machuca, E., Benoit, G., and Antignac, C. (2009). Genetics of nephrotic syndrome: connecting molecular genetics to podocyte physiology. Hum. Mol. Genet. *18* (R2), R185–R194.
10. Mekahli, D., Liutkus, A., Ranchin, B., Yu, A., Bessenay, L., Girardin, E., Van Damme-Lombaerts, R., Palcoux, J.B., Cachat, F., Lavocat, M.P., et al. (2009). Long-term outcome of idiopathic steroid-resistant nephrotic syndrome: a multicenter study. Pediatr. Nephrol. *24*, 1525–1532.
11. Sadowski, C.E., Lovric, S., Ashraf, S., Pabst, W.L., Gee, H.Y., Kohl, S., Engelmann, S., Vega-Warner, V., Fang, H., Halbritter, J., et al.; SRNS Study Group (2015). A single-gene cause in 29.5% of cases of steroid-resistant nephrotic syndrome. J. Am. Soc. Nephrol. *26*, 1279–1289.
12. Kitamura, A., Tsukaguchi, H., Iijima, K., Araki, J., Hattori, M., Ikeda, M., Honda, M., Nozu, K., Nakazato, H., Yoshikawa, N., et al. (2006). Genetics and clinical features of 15 Asian families with steroid-resistant nephrotic syndrome. Nephrol. Dial. Transplant. *21*, 3133–3138.
13. Tsurusaki, Y., Koshimizu, E., Ohashi, H., Phadke, S., Kou, I., Shiina, M., Suzuki, T., Okamoto, N., Imamura, S., Yamashita, M., et al. (2014). De novo SOX11 mutations cause Coffin-Siris syndrome. Nat. Commun. *5*, 4011.
14. Boehmer, T., Jeudy, S., Berke, I.C., and Schwartz, T.U. (2008). Structural and functional studies of Nup107/Nup133 interaction and its implications for the architecture of the nuclear pore complex. Mol. Cell *30*, 721–731.
15. Takai, K., Sawasaki, T., and Endo, Y. (2010). Practical cell-free protein synthesis system using purified wheat embryos. Nat. Protoc. *5*, 227–238.
16. Sawasaki, T., Morishita, R., Gouda, M.D., and Endo, Y. (2007). Methods for high-throughput materialization of genetic information based on wheat germ cell-free expression system. Methods Mol. Biol. *375*, 95–106.
17. Sawasaki, T., Kamura, N., Matsunaga, S., Saeki, M., Tsuchimochi, M., Morishita, R., and Endo, Y. (2008). Arabidopsis HY5 protein functions as a DNA-binding tag for purification and functional immobilization of proteins on agarose/DNA microplate. FEBS Lett. *582*, 221–228.
18. Hawryluk-Gara, L.A., Shibuya, E.K., and Wozniak, R.W. (2005). Vertebrate Nup53 interacts with the nuclear lamina and is required for the assembly of a Nup93-containing complex. Mol. Biol. Cell *16*, 2382–2394.
19. Clever, M., Funakoshi, T., Mimura, Y., Takagi, M., and Imamoto, N. (2012). The nucleoporin ELYS/Mel28 regulates nuclear envelope subdomain formation in HeLa cells. Nucleus *3*, 187–199.
20. Zheng, X., Yang, S., Han, Y., Zhao, X., Zhao, L., Tian, T., Tong, J., Xu, P., Xiong, C., and Meng, A. (2012). Loss of zygotic NUP107 protein causes missing of pharyngeal skeleton and other tissue defects with impaired nuclear pore function in zebrafish embryos. J. Biol. Chem. *287*, 38254–38264.
21. Van Der Spoel, D., Lindahl, E., Hess, B., Groenhof, G., Mark, A.E., and Berendsen, H.J. (2005). GROMACS: fast, flexible, and free. J. Comput. Chem. *26*, 1701–1718.
22. Kelley, L.A., and Sternberg, M.J. (2009). Protein structure prediction on the Web: a case study using the Phyre server. Nat. Protoc. *4*, 363–371.
23. Guerois, R., Nielsen, J.E., and Serrano, L. (2002). Predicting changes in the stability of proteins and protein complexes: a study of more than 1000 mutations. J. Mol. Biol. *320*, 369–387.
24. Bussi, G., Donadio, D., and Parrinello, M. (2007). Canonical sampling through velocity rescaling. J. Chem. Phys. *126*, 014101.
25. Darden, T., York, D., and Pedersen, L. (1993). Particle mesh Ewald: An N·log(N) method for Ewald sums in large systems. J. Chem. Phys. *98*, 10089–10092. http://dx.doi.org/10.1063/1.464397.
26. Hess, B., Bekker, H., Berendsen, H.J.C., and Fraaije, J.G.E.M. (1998). LINCS: A linear constraint solver for molecular simulations. J. Comput. Chem. *18*, 1463–1472, 10.1002/(SICI)1096-987X(199709)18:12<1463:AID-JCC4>3.0.CO;2-H.
27. Banerjee, H.N., Gibbs, J., Jordan, T., and Blackshear, M. (2010). Depletion of a single nucleoporin, Nup107, induces apoptosis in eukaryotic cells. Mol. Cell. Biochem. *343*, 21–25.
28. Antonin, W., Ellenberg, J., and Dultz, E. (2008). Nuclear pore complex assembly through the cell cycle: regulation and membrane organization. FEBS Lett. *582*, 2004–2016.
29. Boehmer, T., Enninga, J., Dales, S., Blobel, G., and Zhong, H. (2003). Depletion of a single nucleoporin, Nup107, prevents the assembly of a subset of nucleoporins into the nuclear pore complex. Proc. Natl. Acad. Sci. USA *100*, 981–985.
30. Hoelz, A., Debler, E.W., and Blobel, G. (2011). The structure of the nuclear pore complex. Annu. Rev. Biochem. *80*, 613–643.
31. Weis, K. (2003). Regulating access to the genome: nucleocytoplasmic transport throughout the cell cycle. Cell *112*, 441–451.
32. Fried, H., and Kutay, U. (2003). Nucleocytoplasmic transport: taking an inventory. Cell. Mol. Life Sci. *60*, 1659–1688.
33. Strambio-De-Castillia, C., Niepel, M., and Rout, M.P. (2010). The nuclear pore complex: bridging nuclear transport and gene regulation. Nat. Rev. Mol. Cell Biol. *11*, 490–501.
34. Ori, A., Banterle, N., Iskar, M., Andrés-Pons, A., Escher, C., Khanh Bui, H., Sparks, L., Solis-Mezarino, V., Rinner, O., Bork, P., et al. (2013). Cell type-specific nuclear pores: a case in point for context-dependent stoichiometry of molecular machines. Mol. Syst. Biol. *9*, 648.
35. Bui, K.H., von Appen, A., DiGuilio, A.L., Ori, A., Sparks, L., Mackmull, M.T., Bock, T., Hagen, W., Andrés-Pons, A., Glavy, J.S., and Beck, M. (2013). Integrated structural analysis of the human nuclear pore complex scaffold. Cell *155*, 1233–1243.
36. Walther, T.C., Alves, A., Pickersgill, H., Loïodice, I., Hetzer, M., Galy, V., Hülsmann, B.B., Köcher, T., Wilm, M., Allen, T., et al. (2003). The conserved Nup107-160 complex is critical for nuclear pore complex assembly. Cell *113*, 195–206.
37. González-Aguilera, C., and Askjaer, P. (2012). Dissecting the NUP107 complex: multiple components and even more functions. Nucleus *3*, 340–348.
38. Mundlos, S., Pelletier, J., Darveau, A., Bachmann, M., Winterpacht, A., and Zabel, B. (1993). Nuclear localization of the protein encoded by the Wilms' tumor gene WT1 in embryonic and adult tissues. Development *119*, 1329–1341.
39. Saotome, I., Curto, M., and McClatchey, A.I. (2004). Ezrin is essential for epithelial organization and villus morphogenesis in the developing intestine. Dev. Cell *6*, 855–864.
40. Thong, K.M., Xu, Y., Cook, J., Takou, A., Wagner, B., Kawar, B., and Ong, A.C. (2013). Cosegregation of focal segmental glomerulosclerosis in a family with familial partial lipodystrophy due to a mutation in LMNA. Nephron Clin. Pract. *124*, 31–37.
41. Nagy, V., Hsia, K.C., Debler, E.W., Kampmann, M., Davenport, A.M., Blobel, G., and Hoelz, A. (2009). Structure of a trimeric

nucleoporin complex reveals alternate oligomerization states. Proc. Natl. Acad. Sci. USA *106*, 17693–17698.
42. Fontoura, B.M., Blobel, G., and Matunis, M.J. (1999). A conserved biogenesis pathway for nucleoporins: proteolytic processing of a 186-kilodalton precursor generates Nup98 and the novel nucleoporin, Nup96. J. Cell Biol. *144*, 1097–1112.
43. Loïodice, I., Alves, A., Rabut, G., Van Overbeek, M., Ellenberg, J., Sibarita, J.B., and Doye, V. (2004). The entire Nup107-160 complex, including three new members, is targeted as one entity to kinetochores in mitosis. Mol. Biol. Cell *15*, 3333–3344.
44. Alber, F., Dokudovskaya, S., Veenhoff, L.M., Zhang, W., Kipper, J., Devos, D., Suprapto, A., Karni-Schmidt, O., Williams, R., Chait, B.T., et al. (2007). Determining the architectures of macromolecular assemblies. Nature *450*, 683–694.
45. Pavenstädt, H., Kriz, W., and Kretzler, M. (2003). Cell biology of the glomerular podocyte. Physiol. Rev. *83*, 253–307.
46. Quaggin, S.E., and Kreidberg, J.A. (2008). Development of the renal glomerulus: good neighbors and good fences. Development *135*, 609–620.
47. Swift, J., and Discher, D.E. (2014). The nuclear lamina is mechano-responsive to ECM elasticity in mature tissue. J. Cell Sci. *127*, 3005–3015.
48. Fedorchak, G.R., Kaminski, A., and Lammerding, J. (2014). Cellular mechanosensing: getting to the nucleus of it all. Prog. Biophys. Mol. Biol. *115*, 76–92.
49. Endlich, N., Kress, K.R., Reiser, J., Uttenweiler, D., Kriz, W., Mundel, P., and Endlich, K. (2001). Podocytes respond to mechanical stress in vitro. J. Am. Soc. Nephrol. *12*, 413–422.
50. Petermann, A.T., Hiromura, K., Blonski, M., Pippin, J., Monkawa, T., Durvasula, R., Couser, W.G., and Shankland, S.J. (2002). Mechanical stress reduces podocyte proliferation in vitro. Kidney Int. *61*, 40–50.
51. Kriz, W. (1996). Progressive renal failure–inability of podocytes to replicate and the consequences for development of glomerulosclerosis. Nephrol. Dial. Transplant. *11*, 1738–1742.
52. Nagata, M., Nakayama, K., Terada, Y., Hoshi, S., and Watanabe, T. (1998). Cell cycle regulation and differentiation in the human podocyte lineage. Am. J. Pathol. *153*, 1511–1520.
53. Alazami, A.M., Patel, N., Shamseldin, H.E., Anazi, S., Al-Dosari, M.S., Alzahrani, F., Hijazi, H., Alshammari, M., Aldahmesh, M.A., Salih, M.A., et al. (2015). Accelerating novel candidate gene discovery in neurogenetic disorders via whole-exome sequencing of prescreened multiplex consanguineous families. Cell Rep. *10*, 148–161.

Clin Exp Nephrol (2015) 19:933–938
DOI 10.1007/s10157-014-1077-8

ORIGINAL ARTICLE

End-stage renal disease in Japanese children: a nationwide survey during 2006–2011

Motoshi Hattori · Mayumi Sako · Tetsuji Kaneko · Akira Ashida · Akira Matsunaga · Tohru Igarashi · Noritomo Itami · Toshiyuki Ohta · Yoshimitsu Gotoh · Kenichi Satomura · Masataka Honda · Takashi Igarashi

Received: 28 September 2014 / Accepted: 17 December 2014 / Published online: 17 January 2015

Abstract
Background End-stage renal disease (ESRD) in children is considered a rare, but serious condition. Epidemiological and demographic information on pediatric ESRD patients around the world is important to better understand this disease and to improve patient care. The Japanese Society for Pediatric Nephrology (JSPN) reported epidemiological and demographic data in 1998. Since then, however, there has been no nationwide survey on Japanese children with ESRD.
Methods The JSPN conducted a cross-sectional nationwide survey in 2012 to update information on the incidence, primary renal disease, initial treatment modalities, and survival in pediatric Japanese patients with ESRD aged less than 20 years during the period 2006–2011.
Results The average incidence of ESRD was 4.0 per million age-related population. Congenital anomalies of the kidney and urinary tract were the most common cause of ESRD, present in 39.8 % of these patients. In addition, 12.2 % had focal segmental glomerulosclerosis and 5.9 % had glomerulonephritis. Initial treatment modalities in patients who commenced renal replacement therapy (RRT) consisted of peritoneal dialysis, hemodialysis, and pre-emptive transplantation (Tx) in 61.7, 16.0, and 22.3 %, respectively. The Japanese RRT mortality rate was 18.2 deaths per 1000 person-years of observation.

On behalf of the Japanese Society for Pediatric Nephrology.

M. Hattori (✉)
Department of Pediatric Nephrology, School of Medicine, Tokyo Women's Medical University, 8-1 Kawada-cho, Shinjuku-ku, Tokyo 162-8666, Japan
e-mail: hattori@kc.twmu.ac.jp

M. Sako
Division for Clinical Trials, Department of Development Strategy, Center for Social and Clinical Research, National Center for Child Health and Development, Tokyo, Japan

T. Kaneko
Division of Clinical Research Support Center, Tokyo Metropolitan Children's Medical Center, Tokyo, Japan

A. Ashida
Department of Pediatrics, Osaka Medical College, Osaka, Japan

A. Matsunaga
Matsunaga Kids Clinic, Yamagata, Japan

T. Igarashi
Department of Pediatrics, Nippon Medical University, Tokyo, Japan

N. Itami
Kidney Center, Nikko Memorial Hospital, Hokkaido, Japan

T. Ohta
Department of Pediatric Nephrology, Hiroshima Prefectural Hospital, Hiroshima, Japan

Y. Gotoh
Department of Pediatrics, Nagoya Daini Red Cross Hospital, Aichi, Japan

K. Satomura
Department of Pediatric Nephrology and Metabolism, Osaka Medical Center and Research Institute for Maternal and Child Health, Osaka, Japan

M. Honda
Department of Nephrology, Tokyo Metropolitan Children's Medical Center, Tokyo, Japan

T. Igarashi
National Center for Child Health and Development, Tokyo, Japan